JOURNAL OF COLLOID AND INTERFACE SCIENCE **182,** 516–525 (1996)
ARTICLE NO. 0496

Dependence of the Far Field Effective Potential on Surface Inhomogeneities

JOHN E. SADER,[1] JAMES S. GUNNING, AND DEREK Y. C. CHAN

Department of Mathematics, University of Melbourne, Parkville, Victoria 3052, Australia

Received December 4, 1995; accepted April 8, 1996

Many surfaces encountered in colloid science are formed by the adsorption of surfactants or polymers on solid surfaces. Due to the formation of surface aggregates, the charge distributions of such surfaces may be nonuniform. Furthermore, these surfaces are expected to have regions with different electrostatic properties due to the presence of two or more different materials. In this paper, we propose a model consisting of periodically alternating regions of constant potential and constant charge, in order to account for the possibility of different regions on the surface possessing different electrostatic properties. Specifically, we consider the behavior of the far field effective electrostatic potential of this model surface when it is immersed in an electrolyte, i.e., the potential associated with the asymptotic exponential tail of the potential distribution in the electrolyte. In doing so, we find the previously unreported phenomenon that the effective potential is strongly dependent on the surface morphology and its associated length scale. Furthermore, we find that there also exists the possibility that the constant charge regions will be "invisible" to the potential distribution. These results have direct implications for general nonuniform charge regulating surfaces.

INTRODUCTION

The electrostatic potential distribution due to a uniformly charged surface has been extensively studied in many geometries, ranging from flat plates to colloidal particles of arbitrary shape. However, many cases occur in practice which violate the fundamental assumption of a uniform surface charge distribution. Such surfaces include those formed by the adsorption of surfactants or polymers on solid surfaces. These surfaces can display nonuniform charge distributions, due to the formation of surface aggregates (1–20). The direct observation of these aggregates has until very recently (19, 20) proven elusive, although their existence has been established by a considerable amount of indirect evidence (1–17). Therefore, the need arises for the study of surfaces with nonuniform surface charge distributions. At this stage we note that this problem has been addressed by a number of workers (21–26). In all these analyses the entire surface was considered to be of the constant charge or constant potential type. However, practical nonuniform surfaces, such as those formed by adsorption, may clearly possess regions with different electrostatic properties, due to the presence of two or more different materials. Therefore, a model which imposes the restriction that the surface is composed of materials of only one type cannot be expected to display all the characteristics of such surfaces. In this paper we consider a surface composed of regions with different electrostatic properties. In particular, we consider a model surface consisting of periodically alternating regions of constant potential and constant charge, which is immersed in an electrolyte. This model is the limiting case of a surface composed of regions which are charge regulating in nature but whose quantitative properties vary spatially. The proposed model displays features which are not present in previous models, and as we shall discuss, gives an indication of what is to be expected from real nonuniform surfaces.

We focus our attention on the far field *effective potential* in the electrolyte, i.e., the potential associated with the asymptotic exponential tail of the potential distribution far from the surface. Schuhmann *et al.* (22) investigated the dependence of the mean surface potential (which is identical to the effective potential in the low potential limit) on surface inhomogeneities of the constant charge type. They found that for large surface potentials, the mean surface potential is dependent on the surface morphology and its associated length scale. The leading order deviation of the mean potential was found to scale with the square of the absolute difference in the surface potentials. However, in the limit of low surface potentials, they found that the effective potential is independent of the length scale associated with the surface morphology, a result consistent with the analysis presented in Ref. (21). This latter result is also true for nonuniform surfaces composed entirely of constant potential regions (23–25). By conducting a detailed analysis of the present model, which consists of regions with different electrostatic properties, we find that the effective potential is in fact strongly dependent on the surface morphology and its associated length scale. We emphasize that this behavior is found

[1] To whom correspondence should be addressed.

0021-9797/96 $18.00

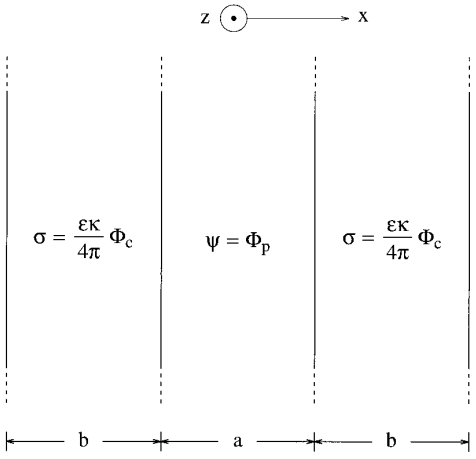

FIG. 1. Schematic depiction of surface showing periodically alternating regions of constant potential and constant charge with boundary conditions, coordinate system, and dimensions indicated. ψ and σ refer to the potential and charge density respectively, ϵ is the relative permittivity of the electrolyte, κ^{-1} is the Debye length, Φ_p and Φ_c are constants, and the period $T \equiv (a + b)$.

in the low potential limit, as we consider only the Debye–Huckel equation, although it is certainly expected to be present for higher potentials as well (25). Furthermore, we find that regimes of surface properties exist in which the constant charge regions will be ''invisible'' to the potential distribution, and we discuss the implications of this finding.

In the next section, we give a detailed statement of the model and the assumptions implicit in our solution. This will be followed by a rigorous analysis of the model, with all details relegated to the Appendixes. Finally, a discussion of the results and their implications shall be given.

MODEL

The model to be considered is a single plate (at $z = 0$) consisting of periodically alternating strips of constant potential and constant charge; see Fig. 1. The governing equation for the potential distribution ψ in the electrolyte ($z > 0$) due to this surface, in the Debye–Huckel approximation, is given by

$$\nabla^2\psi = \kappa^2\psi, \qquad [1]$$

where κ^{-1} is the Debye length. We note that for the present model, the potential distribution decays uniformly and exponentially at large distances from the surface. This asymptotic behavior will be valid provided the distance from the surface is large in comparison to the length scale of the surface distribution. Therefore, we can immediately state that

$$\psi(z) \sim \psi_{\text{eff}} \exp(-\kappa z), \qquad z > O(T), \qquad [2]$$

where T is the period of the repeating regions of constant potential and constant charge (see Fig. 1), and ψ_{eff} is the *effective potential.* The effective potential ψ_{eff} is the primary quantity of interest in this study. Note that at smaller distances from the surface, i.e., $z < O(T)$, the potential distribution will depend on both coordinates x and z (see Fig. 1). The regions $z < O(T)$ and $z > O(T)$ will henceforth be referred to as the *inner region* and *outer region,* respectively.

We initially examine the asymptotic limits where the period T is far greater and far smaller than the Debye length κ^{-1}, for which simple analytic results can be derived. Specifically, we consider the limits of vanishingly small and infinitely large κs, where the normalized period $s = T/2\pi$.

Limit of Vanishing κs

For $\kappa s \ll 1$, the natural length scale for both coordinates x and z close to the surface is the periodicity of the strips. Thus, we scale all lengths by s, and [1] becomes

$$\bar{\nabla}^2\psi = (\kappa s)^2\psi, \qquad [3]$$

where $\bar{\nabla}^2$ is the Laplacian operator scaled by s. Clearly, in the limit $\kappa s \to 0$, [3] reduces to Laplace's equation, $\bar{\nabla}^2\psi = 0$. Note that in the limit of vanishing κs, Laplace's equation is valid only at the surface.

We now examine the boundary conditions at the surface. From Gauss' law, it is clear that the surface charge density σ_{surf} is related to the potential by $\sigma_{\text{surf}} = -(\epsilon/4\pi s)\partial\psi/\partial\bar{z}$, where ϵ is the relative permittivity of the electrolyte solution and $\bar{z} = z/s$ (27). Therefore, in the limit of vanishing κs, it can be easily shown that the appropriate normalized boundary condition in the constant charge region (see Fig. 1) is

$$\left.\frac{\partial\psi}{\partial\bar{z}}\right|_{z=0} = 0. \qquad [4]$$

From Laplace's equation and its associated boundary conditions, it is then clear that the potential distribution on the surface is constant and is simply given by the value of the constant potential regions, i.e., $\psi|_{z=0} = \Phi_p$. The asymptotic expression for the effective potential in the limit of vanishing κs directly follows:

$$\psi_{\text{eff}} = \Phi_p, \quad \kappa s \to 0. \qquad [5]$$

Limit of Infinite κs

In this limiting case, the regions of constant potential and constant charge behave independently from one another. Therefore, their combined contribution to the effective potential can be evaluated by considering the individual regions separately and taking the weighted average of their resulting

potentials in accordance to their geometric ratios. From this we find

$$\psi_{\text{eff}} = \frac{\Phi_p a + \Phi_c b}{a + b}, \quad \kappa s \to \infty, \qquad [6]$$

where $\Phi_c = 4\pi\sigma/\epsilon\kappa$, σ is the charge density in the constant charge regions, and a, b are the geometric parameters defined in Fig. 1.

Comparing the asymptotic results [5, 6], we see that the effective potential ψ_{eff} is in fact a function of κs, and thus a function of the length scale associated with the surface morphology. As we mentioned above, this is in direct contrast to a surface composed entirely of constant potential or constant charge regions, for which the effective potential is independent of κs (see Appendix 1).

Using the inherent linearity of the problem, it is clear from [5, 6] that the effective potential ψ_{eff} may be normalized as

$$\psi_{\text{eff}} = \Phi_p + \frac{b}{a + b}(\Phi_c - \Phi_p) f(\kappa s), \qquad [7]$$

where $f(\kappa s)$ is independent of the surface potentials and charges and has the properties $f(0) = 0$ and $f(\infty) = 1$. Note that $f(\kappa s)$ will also be a function of the surface morphology through its dependence on the geometric parameters a and b. Due to its reduced parameter set, it will be advantageous to consider $f(\kappa s)$ instead of the effective potential ψ_{eff}.

Evaluation for Finite κs

All that remains is the evaluation of the effective potential ψ_{eff} for finite κs. This will be achieved by two independent methods, in order to confirm the validity of the above-mentioned asymptotic results and to check the accuracy of the final results. These methods are (a) a semianalytical method which involves some numerical computations and is capable of achieving accurate results and (b) an approximate analytical method based on a matched asymptotic approach. A brief outline of these two methods will now be given. Those readers interested in their details are referred to Appendixes 2–4.

Semianalytical Method

The general solution to [1] is

$$\psi(\bar{x}, \bar{z}) = \sum_{k=0}^{\infty} A_k \exp\{-\sqrt{1 + (k/\kappa s)^2}\,\bar{z}\} \cos k\bar{x}, \qquad [8]$$

where $\bar{x} = x/s$, $\bar{z} = \kappa z$ (27), and A_k are unknown coefficients which are to be determined by matching the boundary conditions at the surface. We note that these boundary conditions can be represented quite generally as a nonuniform regulation model

$$\alpha(\bar{x})\psi|_{\bar{z}=0} + \beta(\bar{x}) \left.\frac{\partial \psi}{\partial \bar{z}}\right|_{\bar{z}=0} = 1, \qquad [9]$$

where $\alpha(\bar{x})$ and $\beta(\bar{x})$ are functions only of $\bar{x}$. For the present model, these functions are nonzero only within the constant potential and constant charge regions respectively (see Appendix 2 for details).

To evaluate the unknown coefficients A_k, we substitute [8] into [9] and perform a Fourier analysis on the resulting equation. This results in a system of linear equations for the unknown coefficients A_k, which can be solved by standard techniques (28). By definition, the effective potential is given by the mean surface potential. From [8], it is then clear that the effective potential is simply the leading coefficient A_0. From [7], the normalized function $f(\kappa s)$ may then be evaluated:

$$f(\kappa s) = \frac{a + b}{b} \frac{A_0 - \Phi_p}{\Phi_c - \Phi_p}. \qquad [10]$$

Details of the method used to find the coefficient A_0 and hence the function $f(\kappa s)$ are given in Appendix 2. The normalized function $f(\kappa s)$ and the potential distribution ψ can be found to a high precision using this method, the details of which are presented in Appendix 2.

Matched Asymptotic Method

It is possible to obtain a simple yet accurate analytic expression for the normalized function $f(\kappa s)$ using a matched asymptotic analysis. The accuracy of this approach will be tested against the semianalytical method presented above, which is capable of evaluating $f(\kappa s)$ to an arbitrary precision. We shall now give a brief outline of the asymptotic analysis and the main results. Details of this method are given in Appendixes 3 and 4.

The essence of this method is to perform an asymptotic analysis for small and large κs, and then match the resulting expressions to obtain an approximate analytical solution which is valid for all κs. For small κs, a perturbation expansion in terms of κs is performed on the governing Eq. [1] and its associated boundary conditions. This results in a system of governing equations and boundary conditions which are solved using conformal mapping techniques, to obtain a series expansion for $f(\kappa s)$ valid for small κs. For large κs, we use (a) the general solution to [1] given in [8], and (b) the asymptotic result for infinite κs, from which we find $f(\kappa s) = 1 + O((\kappa s)^{-2})$. A Padé approximant (29) is then constructed from the asymptotic expressions for small and large κs, to give a simple analytic expression which is valid for all κs. The result has the form

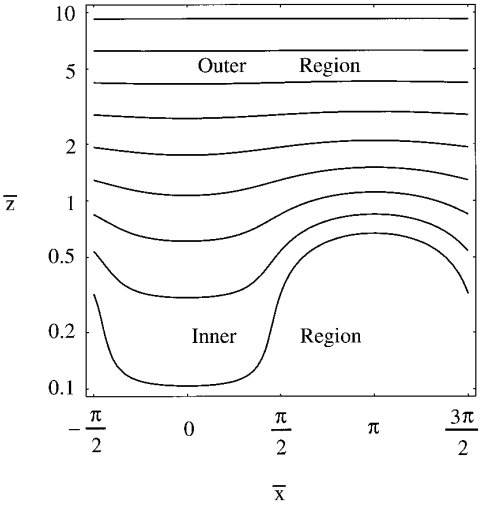

FIG. 2. Plot of equipotential lines for the potential distribution ψ due to a surface with $\pi\kappa s = \kappa T/2 = 1$, $a = b$, $\Phi_p = 1$, $\Phi_c = 3$, evaluated using the semianalytical method with $N = 300$, where $\bar{x} = x/s$ and $\bar{z} = \kappa z$. $\psi_{\text{eff}} = 1.35$. From bottom to top, the equipotential lines are $\psi = 9.05 \times 10^{-1}$, 7.46×10^{-1}, 5.61×10^{-1}, 3.68×10^{-1}, 1.97×10^{-1}, 7.81×10^{-2}, 1.99×10^{-2}, 2.64×10^{-3}, 1.33×10^{-4}. The normalized intervals $[-\pi/2, \pi/2]$ and $[\pi/2, 3\pi/2]$ correspond to the constant potential and constant charge strips, respectively.

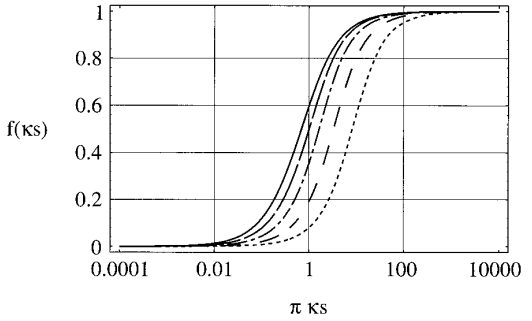

FIG. 3. Normalized function $f(\kappa s)$ defined in [7] obtained using the semianalytical method for various geometric ratios of constant potential/constant charge regions (see Fig. 1). From left to right, $a/T = 0.1$ (solid line); $a/T = 0.25$ (long dash line); $a/T = 0.5$ (short-long dash line); $a/T = 0.75$ (dash line); $a/T = 0.9$ (short dash line).

$$f_{\text{approx}}(\kappa s) = \frac{(a + b)g(\kappa s)}{b + (a + b)g(\kappa s)}, \qquad [11]$$

where

$$g(\kappa s) = \ln\left(\frac{2}{1 - u_c}\right)\left[1 + \kappa s \frac{a}{b} \ln\left(\frac{2}{1 - u_c}\right)\right]\kappa s \qquad [12a]$$

and

$$u_c = \sin\left(\frac{b - a}{b + a}\frac{\pi}{2}\right). \qquad [12b]$$

RESULTS AND DISCUSSION

We now examine the results of the analyses presented in the preceding section and their implications. In Fig. 2, we present a set of generic equipotential lines of ψ, for a specific set of surface parameters, in order to display the properties of the inner and outer regions of the potential distribution. These results were obtained using the semianalytical method presented in Appendix 2. From Fig. 2 it is clear that for $z < O(T)$, corresponding to $\bar{z} \leqslant 2$, there is a strong dependence of the potential distribution on the spatial variable x. However, for $z > O(T)$, corresponding to $\bar{z} \geqslant 2$, this dependence increasingly diminishes with increasing z, until at large distances from the surface the potential distribution is independent of x. It is this far field potential distribution which is under primary investigation in this paper. Note that the qualitative features displayed in Fig. 2 are general properties of the potential distribution.

In Fig. 3, we present results for the normalized function $f(\kappa s)$ as defined in [7], which were obtained numerically using the semianalytical method detailed in the preceding section and in Appendix 2. We note that $f(\kappa s)$ is independent of the values of the surface potentials and charges but is strongly dependent on the surface morphology and its associated length scale s. This dependence on the surface morphology is to be expected, since in the limit $a/T \to 0$ (corresponding to a uniform constant charge surface) $f(\kappa s)$ must approach unity for all finite κs, whereas for $a/T \to 1$ (corresponding to a uniform constant potential surface) $f(\kappa s)$ must approach zero for all finite κs, as is evident from [7]. We also note in Fig. 3 that the function $f(\kappa s)$ behaves as expected in the limits $\kappa s \to 0$ and $\kappa s \to \infty$.

In Fig. 4, we compare the results obtained using the approximate analytical expression [11] to those obtained using the semianalytical method; the difference function $\Delta f =$ Eq. [11] $-$ Eq. [10] is presented. It is evident from Fig. 4 that the approximate expression [11] is quite accurate, with errors

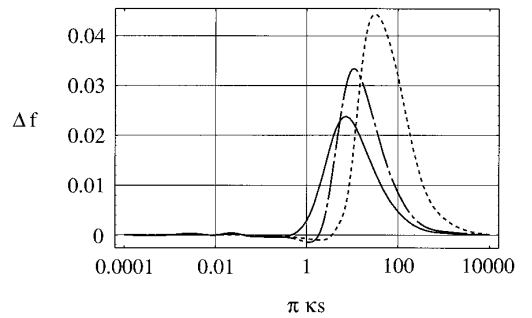

FIG. 4. Difference in approximate expression [11] to the result of the semianalytical method, i.e., $\Delta f =$ Eq. [11] $-$ Eq. [10]. $a/T = 0.1$ (solid line); $a/T = 0.5$ (short-long dash line); $a/T = 0.9$ (short dash line).

less than a few percent for the entire range of κs considered. Furthermore, [11] also matches the asymptotic limits for $\kappa s \to 0$ and $\kappa s \to \infty$, as required.

Note that the asymptotic result [6] for the effective potential, in the infinite κs limit of this model, is identical to that of a nonuniform surface composed entirely of constant potential or constant charge regions (see Appendix 1). This is to be expected, since (a) for all models the effective potential is given by the mean surface potential, (b) for surfaces composed entirely of either constant potential or constant charge regions, the effective potential is independent of κs (see Appendix 1), and (c) as far as the effective potential is concerned, the present model is identical to the surfaces discussed in (b) for the infinite κs limit, since the individual regions behave independently of one another.

The implications of these results are quite striking. We see that in the limit of vanishing κs, the constant charge regions are in fact invisible to the potential distribution. The surface therefore behaves as a uniform constant potential surface, with a surface potential equal to that of the constant potential regions, namely Φ_p. Note that this result is independent of the surface morphology through its independence on the geometric parameters a and b. As κs is increased, a monotonic increase in the importance of the constant charge regions is observed, until the limit of infinite κs is attained, where the constant potential and constant charge regions contribute proportionally to the effective potential according to their geometric ratios. This is in direct contrast to surfaces composed entirely of constant potential (or charge) regions, for which the effective potential is independent of κs and is simply given by the area average of the individual strip potentials, if they were taken in isolation (see Appendix 1).

All features and phenomena found in the present one dimensional strip model are also expected to be found when generalized to a two dimensional surface distribution, since the basic physical origin of these phenomena is identical in both cases and is directly linked to the interaction between the potential and charge determining properties of the surface. Also, we note that the present model is in fact an example of a nonuniform charge regulating surface and is simply a limiting case of the general problem, as is evident from [9]. Since a general nonuniform charge regulating surface also allows such an interaction between its charge and potential determining properties, it is expected that the phenomena found for the present model should also be present in all nonuniform charge regulating surfaces.

These results indicate the very interesting possibility that a constant potential-like surface modified by the adsorption of a surfactant will electrostatically behave in an identical manner to the original surface, provided the length scale of the surfactant distribution is far smaller than the Debye length. Furthermore, these results indicate that the far field electrostatic behavior of a surface with a given surface morphology and associated length scale, can be very different to a surface with the same morphology but with a different length scale.

CONCLUSIONS

Previous theoretical models of nonuniformly charged surfaces have considered the entire surface to be of the constant potential or the constant charge type. However, many nonuniformly charged surfaces encountered in practice are expected to possess regions with different electrostatic properties, due to the presence of two or more different materials. To examine the effect of these types of nonuniformities, we proposed a simple model consisting of a mixture of regions of constant potential and constant charge. In so doing, we found that the effective potential is strongly dependent on the length scale associated with the surface morphology, a phenomenon which (a) is not predicted by previous theoretical models for nonuniform surfaces, and (b) should also be found in general nonuniform charge regulating surfaces. Furthermore, we found that in the limit of vanishingly small κs, the constant charge regions are invisible to the potential distribution, irrespective of their fractional area of coverage. This indicates the possibility that an adsorbed surfactant can be invisible or have little effect on the electrostatic properties of the surface.

A1. APPENDIX 1

In this appendix, we give the exact analytical expression for the potential distribution due to a single plate composed of (a) periodically alternating constant potential strips and (b) periodically alternating constant charge strips, which is immersed in an electrolyte. The geometry of the plate is identical to that presented in Fig. 1, but the boundary conditions differ. In particular, for the constant potential type plate, the strips of width a and b have fixed potentials of Φ_1 and Φ_2, respectively, whereas for the constant charge type plate, the strips of width a and b have fixed charge densities of σ_1 and σ_2, respectively.

We begin by noting that the general solution to [1] is

$$\psi(\bar{x}, \bar{z}) = \sum_{n=0}^{\infty} C_n \exp\{-\sqrt{1 + (n/\kappa s)^2}\, \bar{z}\} \cos n\bar{x}, \quad [A1\text{-}1]$$

where C_n are unknown coefficient to be determined, and $\bar{x} = x/s, \bar{z} = \kappa z$. The periodic boundary condition at the surface is then expressed as a Fourier series. At the surface this series must match that obtained using [A1-1]; this directly gives the coefficients C_n. For the constant potential plate, we then find

$$C_n = \begin{cases} \dfrac{a\Phi_1 + b\Phi_2}{a+b}, & n = 0 \\ \dfrac{2(\Phi_1 - \Phi_2)}{n\pi} \sin\left(n\pi \dfrac{a}{a+b} \right), & \text{otherwise,} \end{cases} \quad [A1\text{-}2]$$

whereas for the constant charge type plate

$$C_n = \frac{4\pi}{\epsilon\kappa} \sqrt{1 + (n/\kappa s)^2} \begin{cases} \dfrac{a\sigma_1 + b\sigma_2}{a+b}, & n = 0 \\ \dfrac{2(\sigma_1 - \sigma_2)}{n\pi} \sin\left(n\pi \dfrac{a}{a+b} \right), & \text{otherwise.} \end{cases} \quad [A1\text{-}3]$$

Note that in both cases the effective potential, as given by C_0, is independent of κs, a result which is well known for these types of surfaces (21–25).

A2. APPENDIX 2

In this appendix, we give the details of a semianalytical method of solution for the Debye–Huckel equation [1]. We begin by noting that the general solution of [1] for the present model is

$$\psi(\bar{x}, \bar{z}) = \sum_{k=0}^{\infty} A_k \exp\{-\sqrt{1 + (k/\kappa s)^2}\, \bar{z}\} \cos k\bar{x}, \quad [A2\text{-}1]$$

where A_k are unknown coefficients to be determined, and $\bar{x} = x/s$, $\bar{z} = \kappa z$. The boundary conditions at the surface in the individual regions of the present model (see Fig. 1) are then represented as a nonuniform regulation model,

$$\alpha(\bar{x})\psi|_{\bar{z}=0} + \beta(\bar{x}) \left. \frac{\partial \psi}{\partial \bar{z}} \right|_{\bar{z}=0} = 1, \quad [A2\text{-}2]$$

where

$$\alpha(\bar{x}) = \begin{cases} \Phi_p^{-1}, & \text{in constant potential regions} \\ 0, & \text{otherwise,} \end{cases} \quad [A2\text{-}3a]$$

$$\beta(\bar{x}) = \begin{cases} -\Phi_c^{-1} \equiv -\dfrac{\epsilon\kappa}{4\pi\sigma}, & \text{in constant charge regions} \\ 0, & \text{otherwise.} \end{cases} \quad [A2\text{-}3b]$$

To evaluate the unknown coefficients A_k, the infinite series in [A2-1] is first truncated at some upper limit $k = N$ and then substituted into [A2-2]. The resulting expression is multiplied by $\cos n\bar{x}$, where $n = 0, \ldots, N$, and integrated over one period of the surface, i.e., $\bar{x} \in [0, 2\pi]$. Use is then made of the orthogonality properties of trigonometric functions, from which a system of linear equations in the unknowns A_k results. The solution of this system is

$$\mathbf{A} = \mathbf{M}^{-1}\mathbf{F}, \quad [A2\text{-}4]$$

where $\mathbf{A} = [A_0, A_1, \ldots, A_N]^{\mathrm{T}}$ is a column vector in the unknown coefficients, $\mathbf{F} = [2\pi, 0, 0, \ldots, 0]^{\mathrm{T}}$ is a column vector with only one nonzero element, and the elements of the matrix $\mathbf{M}$ are given by

$$M_{ij} = \Phi_p^{-1} I\left(i, j, -\frac{\bar{a}}{2}, \frac{\bar{a}}{2} \right) - \Phi_c^{-1} I\left(i, j, \frac{\bar{a}}{2}, \frac{\bar{a}}{2} + \bar{b} \right), \quad [A2\text{-}5]$$

where $\bar{a} = a/s$, $\bar{b} = b/s$ and $i, j = 0, \ldots, N$. The function $I(i, j, r, t)$ is given by

$$I(i, j, r, t) = \begin{cases} \dfrac{(\sin[t(i-j)] - \sin[r(i-j)])}{2(i-j)} + \dfrac{(\sin[t(i+j)] - \sin[r(i+j)])}{2(i+j)}, & i \neq j \\ \dfrac{t-r}{2} + \dfrac{\sin(2ti) - \sin(2ri)}{4i}, & i = j \neq 0 \\ t - r, & i = j = 0. \end{cases} \quad [A2\text{-}6]$$

The effective potential ψ_{eff} is given by the leading coefficient A_0. This result is substituted into [7], from which the final expression for the normalized function $f(\kappa s)$ directly follows,

$$f(\kappa s) = \frac{a+b}{b} \frac{A_0 - \Phi_p}{\Phi_c - \Phi_p}. \quad [A2\text{-}7]$$

In the numerical evaluation of $f(\kappa s)$, it was found that approximately 300 terms in the expansion were required to attain a convergence of 0.1%.

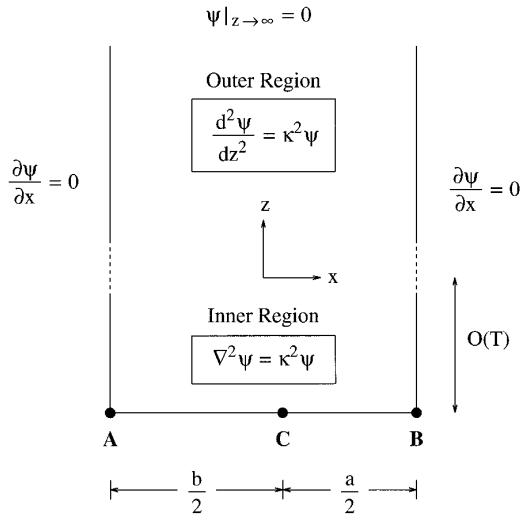

FIG. 5. One period of surface displaying inner and outer regions. Governing equations (boxed), boundary conditions (unboxed). Origin of coordinate system is midway along A–B.

A3. APPENDIX 3

In this appendix, we give the derivation of the approximate analytical result [11]. We begin by considering the solution for small but finite κs, i.e., $\kappa s \ll 1$. As was discussed above, the structure in the potential distribution with respect to x, is only observed for $z < O(T)$, e.g., see Fig. 2. For $\kappa s \ll 1$, it is then clear that there exists a thin boundary layer next to the surface where there is rapid x-variation in the potential. Outside this boundary layer the potential is essentially only a function of z. The graphical representation of this problem is given in Fig. 5.

Within the boundary layer, previously referred to as the *inner region* (see Fig. 5), the appropriate length scale for both x and z is s. Therefore, we expand ψ in a power series of κs,

$$\psi(\bar{x}, \bar{z}) = \sum_{n=0}^{\infty} (\kappa s)^n \psi_n(\bar{x}, \bar{z}), \qquad [A3\text{-}1]$$

where $\bar{x} = x/s$ and $\bar{z} = z/s$ (27). We retain this scaling for z throughout this appendix and its associated diagrams. Substituting [A3-1] into [3] and the boundary conditions at $z = 0$, and equating terms of equal order results in the system of equations for the unknowns ψ_n

$$\bar{\nabla}^2\psi_n = \psi_{n-2}, \quad n \geq 0, \qquad [A3\text{-}2]$$

where $\psi_n = 0$ if $n < 0$. The associated boundary conditions for the constant potential regions are

$$\bar{\Phi}_n \equiv \psi_n\Big|_{z=0} = \begin{cases} \Phi_p, & n = 0 \\ 0, & \text{otherwise,} \end{cases} \qquad [A3\text{-}3a]$$

whereas for the constant charge regions we have

$$\bar{\sigma}_n \equiv \frac{\partial\psi_n}{\partial\bar{z}}\Big|_{z=0} = \begin{cases} -\Phi_c, & n = 1 \\ 0, & \text{otherwise.} \end{cases} \qquad [A3\text{-}3b]$$

The solution in the region outside the boundary layer, previously referred to as the *outer region* (see Fig. 5), is given by

$$\psi(\bar{z}) = \psi_{\text{eff}} \exp(-\kappa s\bar{z}), \qquad [A3\text{-}4]$$

where

$$\psi_{\text{eff}} = \sum_{n=0}^{\infty} (\kappa s)^n B_n. \qquad [A3\text{-}5]$$

The coefficients B_n are yet to be determined and are independent of κs. [A3-5] accounts for the variation in the effective potential with κs. Expanding [A3-4] in a power series in κs, we find

$$\psi(\bar{z}) = \sum_{n=0}^{\infty} (\kappa s)^n \Omega_n(\bar{z}), \qquad [A3\text{-}6]$$

where

$$\Omega_n(\bar{z}) = \sum_{m=0}^{n} \frac{(-1)^m \bar{z}^m}{m!} B_{n-m}. \qquad [A3\text{-}7]$$

By solving [A3-2] in the inner region and matching the result to the solution in the outer region [A3-6], the effective potential can be determined using [A3-5].

We now turn our attention to the solution in the inner region. The general problem to be solved is illustrated in Fig. 6. We begin by considering the zeroth order term ψ_0.

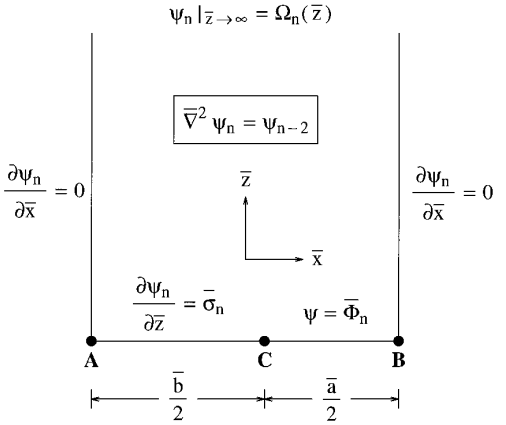

FIG. 6. Schematic definition of problem for the inner region. Governing equation (boxed), boundary conditions (unboxed). Origin of coordinate system is midway along A–B. Functions scaled by s are indicated with an over bar. $\bar{\Phi}_n$ and $\bar{\sigma}_n$ are defined in [A3-3a] and [A3-3b], respectively.

Zeroth Order Term ψ_0

It is clear from Fig. 6 that the solution to ψ_0 is

$$\psi_0(\bar{x}, \bar{z}) = \Phi_p. \qquad [A3\text{-}8]$$

Equating [A3-8] and $\Omega_0(\bar{z})$ then gives

$$B_0 = \Phi_p, \qquad [A3\text{-}9]$$

which is the required asymptotic result [5].

First Order Term ψ_1

Due to complications in the boundary conditions, the solution of the first order term poses a greater challenge than that of the zeroth order term. We note that the problem for ψ_1 is similar to the problem solved in Appendix 4, the differences being that (a) not all the boundary conditions at $\bar{z} = 0$ are zero, and (b) the lengths of the base lines at $\bar{z} = 0$ are not identical.

To eliminate the nonzero boundary condition along $A-C$ in Fig. 6, we define a function ϕ_1 such that

$$\phi_1 = \psi_1 + \Phi_c \bar{z}. \qquad [A3\text{-}10]$$

The governing equation for ϕ_1 is then found by substituting [A3-10] into the governing equation for ψ_1, from which we find Laplace's equation,

$$\bar{\nabla}^2 \phi_1 = 0. \qquad [A3\text{-}11]$$

The base length for the present problem can be made identical to that in Appendix 4, by applying a linear transformation to map the interval $[-(a + b)/4, (a + b)/4]$ to $[-\pi/2, \pi/2]$. Using all the above mentioned transformations and solving for ϕ_1, it can be easily shown using the result of Appendix 4 that the solution to the first order term is given by

$$\psi_1(\bar{x}, \bar{z}) = -\Phi_c \bar{z} - (\Phi_p - \Phi_c)\mathrm{Im}\left\{ \sin^{-1} \times \left[\frac{2 \sin(\bar{x} + i\bar{z}) - 1 - u_c}{1 - u_c} \right] \right\}, \qquad [A3\text{-}12]$$

where

$$u_c = \sin\left(\frac{b - a}{b + a} \frac{\pi}{2} \right). \qquad [A3\text{-}13]$$

Taking the asymptotic limit of [A3-12] as $\bar{z} \to \infty$, and matching this to $\Omega_1(\bar{z})$, we then find

$$B_1 = (\Phi_p - \Phi_c) \ln\left(\frac{1 - u_c}{2} \right). \qquad [A3\text{-}14]$$

Second Order Term ψ_2

The solution to ψ_2 is evaluated in an analogous manner to that for ψ_1, the difference being that we do not modify the boundary conditions at $\bar{z} = 0$, but instead modify the boundary conditions at $\bar{z} = \infty$. We achieve this by defining a function ϕ_2 such that

$$\phi_2 = \psi_2 - \frac{\Phi_p \bar{z}^2}{2}. \qquad [A3\text{-}15]$$

The governing equation for ϕ_2 is then found by substituting [A3-15] into the governing equation for ψ_2, from which we find that ϕ_2 satisfies Laplace's equation. We also see that the boundary conditions for ϕ_2 are identical to the problem presented in Appendix 4.

The length of the base $A-B$ is again transformed to match the length of the problem in Appendix 4, using the same linear transformation as specified in the solution of ψ_1. Applying all the above transformations reduces the original problem into that presented in Appendix 4. Using the result in Appendix 4, we then find the required solution for ψ_2,

$$\psi_2(\bar{x}, \bar{z}) = \frac{\Phi_p \bar{z}^2}{2} - B_1 \mathrm{Im}\left\{ \sin^{-1} \times \left[\frac{2 \sin(\bar{x} + i\bar{z}) - 1 - u_c}{1 - u_c} \right] \right\}. \qquad [A3\text{-}16]$$

Taking the asymptotic limit of [A3-16] as $\bar{z} \to \infty$ and matching this to $\Omega_2(\bar{z})$, we find

$$B_2 = (\Phi_p - \Phi_c) \ln^2\left(\frac{1 - u_c}{2} \right). \qquad [A3\text{-}17]$$

Substituting [A3-9], [A3-14], and [A3-17] into [A3-5] gives the effective potential correct to $O((\kappa s)^2)$. Substituting the resulting expression into [7], we find that the normalized function $f(\kappa s)$ is

$$f(\kappa s) = -\frac{a + b}{b} \ln\left(\frac{1 - u_c}{2} \right) \times \left[1 + \kappa s \ln\left(\frac{1 - u_c}{2} \right) \right] \kappa s + O((\kappa s)^3). \qquad [A3\text{-}18]$$

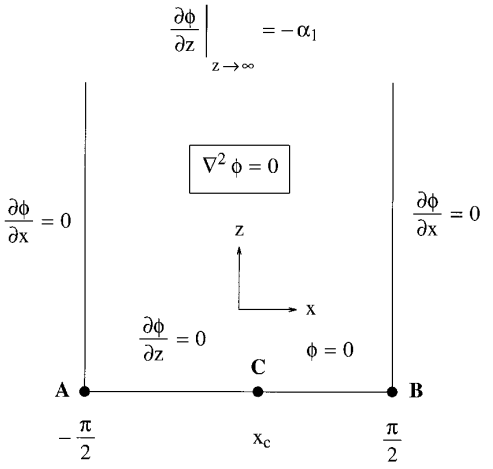

FIG. 7. Schematic definition of problem posed in Appendix 4. Governing equation (boxed), boundary conditions (unboxed). Origin of coordinate system is midway along A–B. $x_c = \sin^{-1} u_c$.

With the solution for small κs evaluated, correct to $O((\kappa s)^2)$, we turn our attention to the asymptotic solution for large κs. As discussed above, the asymptotic form of $f(\kappa s)$ for large κs is

$$f(\kappa s) = 1 + O\left(\frac{1}{(\kappa s)^2}\right). \qquad [A3\text{-}19]$$

Using the theory of Padé approximants (29), we now formulate an approximate analytical result, valid for all κs, from the asymptotic forms of $f(\kappa s)$ for small and large κs. From [A3-18] and [A3-19] we find

$$f_{\text{approx}}(\kappa s) = \frac{(a+b)g(\kappa s)}{b + (a+b)g(\kappa s)}, \qquad [A3\text{-}20]$$

where

$$g(\kappa s) = \ln\left(\frac{2}{1-u_c}\right)\left[1 + \kappa s \frac{a}{b}\ln\left(\frac{2}{1-u_c}\right)\right]\kappa s. \qquad [A3\text{-}21]$$

A4. APPENDIX 4

In this Appendix, we give the solution to Laplace's equation with the domain and boundary conditions depicted in Fig. 7. This result is used in Appendix 3 in the evaluation of [11]. The conformal mapping technique (30) lends itself ideally to the solution of this problem since (a) the problem is two dimensional and (b) the boundary conditions are homogeneous. The most appropriate transformation for this problem is the mapping

$$w = \sin y, \qquad [A4\text{-}1]$$

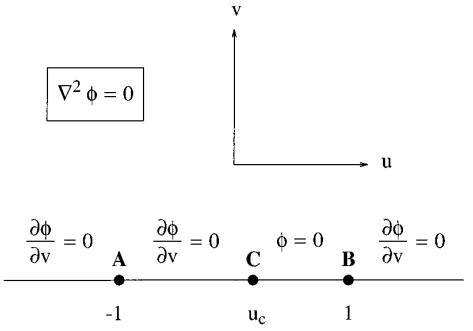

FIG. 8. Conformal mapping of problem depicted in Fig. 7 using $w = \sin y$, where $w = u + iv$. Governing equation (boxed), boundary conditions (unboxed). Origin of coordinate system is midway along A–B.

where $y = x + iz$. This transforms the ''potential well'' problem in Fig. 7 to that of a straight line, as depicted in Fig. 8. The interval C–B in Fig. 8 is further mapped to the interval $[-1, 1]$, using the linear transformation

$$\hat{w} = \frac{2w - 1 - u_c}{1 - u_c}. \qquad [A4\text{-}2]$$

Applying the inverse mapping $\hat{y} = \sin^{-1}\hat{w}$ to the resulting problem gives Fig. 9. We note that in all the above transformations and mappings, the boundary conditions remain unchanged. Using this property, it is then clear that the solution to the problem depicted in Fig. 9 is

$$\phi = -\alpha_1 \text{Im}\{\hat{y}\}. \qquad [A4\text{-}3]$$

Using [A4-2] and taking into account all the conformal mappings and transformations used, it may then be easily shown from [A4-3] that the required solution is

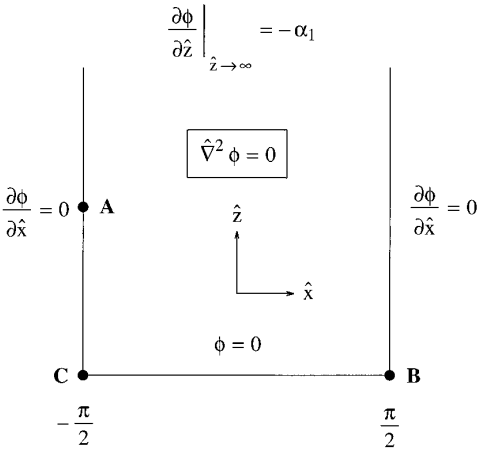

FIG. 9. Conformal mapping of problem depicted in Fig. 8 using $\hat{y} = \sin^{-1}\hat{w}$ and the transformation [A4-2], where $\hat{y} = \hat{x} + i\hat{z}$. Governing equation (boxed), boundary conditions (unboxed). Origin of coordinate system is midway along C–B.

$$\phi(x, z) = -\alpha_1 \mathrm{Im}\left\{ \sin^{-1}\left[\frac{2 \sin(x + iz) - 1 - u_c}{1 - u_c} \right] \right\}. \quad [A4\text{-}4]$$

ACKNOWLEDGMENTS

This research was funded in part by an Australian Research Council Grant (A69230979) and by the Advanced Minerals Products Centre, an ARC special research centre.

REFERENCES

1. Gaudin, A. M., and Fuerstenau, D. W., *Trans. AIME* **202,** 958 (1955).
2. Somasundaran, P., Healy, T. W., and Fuerstenau, D. W., *J. Phys. Chem.* **68,** 3562 (1964).
3. Somasundaran, P., and Fuerstenau, D. W., *J. Phys. Chem.* **70,** 90 (1966).
4. Waterman, K. C., Turro, N. J., Chandar, P., and Somasundaran, P., *J. Phys. Chem.* **90,** 6828 (1986).
5. Chandar, P., Somasundaran, P., and Turro, N. J., *J. Colloid Interface Sci.* **117,** 31 (1987).
6. Somasundaran, P., and Kunjappu, J. T., *Colloids Surf.* **37,** 245 (1989).
7. Kunjappu, J. T., and Somasundaran, P., *J. Colloid Interface Sci.* **175,** 520 (1995).
8. Levitz, P., El Miri, A., Keravis, D., and Van Damme, H., *J. Colloid Interface Sci.* **99,** 484 (1984).
9. Levitz, P., Van Damme, H., and Keravis, D., *J. Phys. Chem.* **88,** 2228 (1984).
10. Levitz, P., and Van Damme, H., *J. Phys. Chem.* **90,** 1302 (1986).
11. Partyka, S., Zaini, S., Lindheimer, M., and Brun, B., *Colloid Surface* **12,** 255 (1984).
12. Lindheimer, M., Keh, E., Zaini, S., and Partyka, S., *J. Colloid Interface Sci.* **138,** 83 (1990).
13. Bohmer, M. R., Koopal, L. K., Jansen, R., Lee, E. M., Thomas, R. K., and Rennie, A. R., *Langmuir* **8,** 2228 (1992).
14. Rutland, M. W., and Parker, J. L., *Langmuir* **10,** 1110 (1994).
15. Giordano-Palmino, F., Denoyel, R., and Rouquerol, J., *J. Colloid Interface Sci.* **165,** 82 (1994).
16. Cummins, P. G., Staples, E., and Penfold, J., *J. Phys. Chem.* **94,** 3740 (1990).
17. Soderman, O., and Stilbs, P., *Prog. Nucl. Magn. Reson. Spectrosc.* **26,** 445 (1994).
18. Rupprecht, H., and Gu, T., *Colloid Polym. Sci.* **269,** 506 (1991).
19. Hayes, K. F., and Morton, J. D., ''Atomic Force Microscopy Studies of Cetyltrimethylammonium Sorption at Mineral/Water Interfaces,'' presented at ACS Colloid and Interface Science Symposium, Stanford University, July 1994.
20. Nishimura, S., Scales, P. J., Biggs, S. R., and Healy, T. W., *Colloids Surf. A Physicochem. Eng. Aspects* **103,** 289 (1995).
21. Richmond, P., *J. Chem. Soc. Faraday Trans. 2* **70,** 1066 (1974).
22. Schuhmann, D., and D'Epenoux, B., *J. Colloid Interface Sci.* **116,** 159 (1987).
23. Kuin, A. J., *Faraday Discuss. Chem. Soc.* **90,** 235 (1990).
24. Vreeker, R., Kuin, A. J., Den Boer, D. C., Hoekstra, L. L., and Agterof, W. G. M., *J. Colloid Interface Sci.* **154,** 138 (1992).
25. Miklavic, S. J., Chan, D. Y. C., White, L. R., and Healy, T. W., *J. Phys. Chem.* **98,** 9022 (1994).
26. Grant, M. L., and Saville, D. A., *J. Colloid Interface Sci.* **171,** 35 (1995).
27. Two different scalings for z are used in this paper, namely $\bar{z} = z/s$ and $\bar{z} = \kappa z$. The first is used when considering the solution near the surface for $\kappa s \ll 1$, since s is the natural length scale there, whereas the second is used when considering the general solution to [1] at all distances from the plate and for all κs. The use of one or the other of these scalings is indicated in the text to avoid confusion.
28. Hornbeck, R. W., ''Numerical Methods,'' Quantum, New York, 1975.
29. Bender, C. M., and Orszag, S. A., ''Advanced Mathematical Methods for Scientists and Engineers,'' McGraw–Hill, Singapore, 1978.
30. Churchill, R. V., Brown, J. W., and Verhey, R. F., ''Complex Variables and Applications,'' McGraw–Hill, New York, 1974.